Earthq Eng & Eng Vib (2013) 12: 473-486 **DOI**: 10.1007/s11803-013-0187-8

Soil bentonite wall protects foundation from thrust faulting: analyses and experiment

M. Fadaee[1†], I. Anastasopoulos[2‡], G. Gazetas[2§], M.K. Jafari[1§] and M. Kamalian[1*]

1. *International Institute of Earthquake Engineering and Seismology, Tehran, Iran*

2. *School of Civil Engineering, National Technical University, Athens, Greece*

Abstract: When seismic thrust faults emerge on the ground surface, they are particularly damaging to buildings, bridges and lifelines that lie on the rupture path. To protect a structure founded on a rigid raft, a thick diaphragm-type soil bentonite wall (SBW) is installed in front of and near the foundation, at sufficient depth to intercept the propagating fault rupture. Extensive numerical analyses, verified against reduced–scale (1 g) split box physical model tests, reveal that such a wall, thanks to its high deformability and low shear resistance, "absorbs" the compressive thrust of the fault and forces the rupture to deviate upwards along its length. As a consequence, the foundation is left essentially intact. The effectiveness of *SBW* is demonstrated to depend on the exact location of the emerging fault and the magnitude of the fault offset. When the latter is large, the unprotected foundation experiences intolerable rigid-body rotation even if the foundation structural distress is not substantial.

Keywords: soil bentonite wall; fault rupture; soil-structure interaction; seismic hazard; mitigation; tectonic deformation; soil-foundation interaction

1 Introduction

Thrust-fault seismic events have repeatedly revealed the damage potential from fault breakout on the ground surface: structures straddling the rupture can be subjected to intolerable differential displacements. The recent Chi-Chi (1999) and Wenchuan (2008) earthquakes offered numerous examples of severe damage to a variety of structures located over the outcrop of thrust faults. Some examples of such severe damage due to thrust faulting are given in Fig. 1 (photos adapted from Lin *et al*., 2009). Specifically, in the M_w 7.6 Chi-Chi earthquake, the seismogenic Chelongpu fault, with a total length of over 90 km, propagated all the way to the ground surface, generating a multitude of fault scarps of vertical offset that reached a colossal 10 m. Buildings, bridges, a concrete dam, electric pylons, pipelines, and retaining walls, crossed by the fault, provided well-documented case histories of fault rupture interaction with engineered structures (e.g., Faccioli *et al*., 2008). One such example is shown in Fig. 1(a), depicting a severely damaged 2-story building, which was subjected to a fault offset of approximately 1.5 m.

Equally spectacular were the case histories from the devastating M_w 7.8 2008 Wenchuan earthquake in China. Three parallel seismic faults emerged on the ground surface for a total length of 280 km – one of the longest in record (Lin *et al*., 2009) with up to 6 m of permanent vertical ground displacement in addition to some smaller horizontal components. The fault crossed several urban areas, inflicting damage to bridges, lifelines, and buildings. One such example is portrayed in Fig. 1(b), which shows the partial collapse of a 3-story building subjected to a fault offset of approximately 1 m (Lin *et al*., 2009).

Research efforts combining field studies (Anastasopoulos and Gazetas, 2007a; Faccioli *et al*., 2008), centrifuge model tests (Bransby *et al*., 2008), and theoretical analyses (Anastasopoulos and Gazetas, 2007b; Anastasopoulos *et al*., 2008 and 2009; Paolucci and Yilmaz, 2008) have culminated in the development of a validated methodology for analysis and design of foundation–structure systems against faulting-induced deformation. It has been shown that the movement and distress of a structure depend on the interplay between the deforming soil and the foundation–structure system. The type of foundation proved to play a crucial role in the survival of a structure. Especially when heavily loaded, continuous and rigid foundation systems (such as slab or box-type foundations) may lead to fault rupture diversion.

Correspondence to: Meysam Fadaee, International Institute of Seismology and Earthquake Engineering, No. 21, Arghavan St., North Dibajee, Farmanieh, Tehran, Iran
Tel: +9821-22830830; Fax: +9821-22299479
E-mail: m.fadaie@iiees.ac.ir

[†]PhD, Research Assistant; [‡]Assistant Professor; [§]Professor; [*]Associate Professor

Received October 2, 2012; **Accepted** March 18, 2013

Fig. 1 Examples of structural damage due to reverse faulting: (a) severe damage of a 2-story building subjected to a fault offset of about 1.5 m during the 1999 Chi-Chi earthquake; (b) partial collapse of a 3-story building, subjected to a fault offset of about 1 m during the 2008 Wenchuan earthquake in China (adapted from Lin *et al*., 2009)

Even with a partial diversion, such foundations impose kinematic constraints, "flattening" the faulting–induced ground deformation and allowing the structure to rotate as a rigid body. Although foundations may experience loss of support, a continuous and rigid foundation could perform as a cantilever or a simply supported beam, bridging the locally generated gaps and drastically reducing the distress of the superstructure. Nevertheless, even rigid body rotation may condemn the operation of a facility.

Such methods have been applied to design soil–structure systems to sustain large tectonic deformation in several major projects, including: the buildings of a housing complex and of a luxury resort, a 400 m viaduct bridge, cut–and–cover and lane–cover tunnels, several highway bridges of a major highway, and a deep immersed tunnel (Anastasopoulos and Gazetas, 2005 and 2010; Anastasopoulos *et al*., 2008a and 2008b). In buildings, although a rigid and continuous foundation system can easily be applied for new structures, it is neither straightforward nor cost effective to retrofit existing ones. Especially for historic buildings and monuments, the addition of a continuous and rigid foundation may be practically impossible. Moreover, even if such retrofit were possible, the rotation of the structure as a rigid body would not be avoided – something which may not be acceptable. Such structures, built centuries ago, can be situated in the immediate vicinity or on top of active seismic faults covered with soil. Even if avoidance was an option for new structures (it usually is not, as the exact location of a fault emergence cannot be known a-priori with accuracy), it is obviously out of the question for existing structures and monuments. Hence, there is a necessity to devise efficient faulting hazard mitigation schemes, preferably ones that require minimum intervention.

This paper explores a novel technique to protect civil engineering structures from thrust faulting. Instead of strengthening the foundation (and/or the superstructure) to sustain the imposed tectonic deformation, the proposed seismic hazard mitigation technique aims at diverting the fault rupture, so that the structure remains practically unaffected from the tectonic deformation. This is achieved through construction of a wall "barrier" placed between the outcropping dislocation and the foundation–structure system. Since the rupture will propagate along a path of least effort (Berill, 1983; Yilmaz and Paolucci, 2007), the proposed "barrier" is weaker and softer than the surrounding soil layers, acting as an "attractor" of the imposed plastic shearing

Fig. 2 Soil bentonite wall (SBW) under construction: (a) distant view; and (b) close view (adapted from McKnight *et al.*, 2001)

deformation and as a "fuse" that absorbs the imposed passive-type compression. As will be discussed in detail, the weak and soft wall "barrier" can be materialized through a *Soil Bentonite Wall* (SBW).

Such walls are constructed using standard diaphragm wall machinery (Fig. 2), and are typically used as a cost–efficient low–permeability diaphragm to control seepage under embankment dams and landfill leakage (McKnight *et al.*, 2001; Ryan, 2007), or for environmental protection purposes (e.g., to avoid diffusion of contaminants). Their shear strength is lower than that of the surrounding soil, due to: (a) the construction method – the natural soil is extracted, and then backfilled without any compaction; (b) the stress conditions after backfilling of the trench – substantially less than the geostatic due to arching effect; and (c) the constituent material – the backfilling is a mixture of natural soil, bentonite, and water (Evan *et al*., 1995; Baxter, 2000).

Combining low shear strength, high compressibility, ease of construction, and cost–effectiveness, the SBW can be seen as a valid choice to construct such a fault "barrier." Naturally, various other mitigation techniques may also be applicable (see Bray, 2001), but are beyond the scope of this paper.

2 Problem definition and methodology

The aim of this paper is to demonstrate the effectiveness of the SBW for surface foundations subjected to thrust faulting. The problem is schematically illustrated in Fig. 3. A uniform soil deposit of depth H = 20 m is considered, at the base of which a thrust fault with a dip angle $\alpha = 45^{o}$ produces upward displacement of vertical amplitude h. A stiff raft foundation of width B = 10 m carrying a surcharge load q, is positioned at distance s from the theoretical point of rupture outcropping in the free field (i.e., unperturbed from foundation). To assess the effectiveness of the proposed mitigation scheme, the untreated case (i.e., without any mitigation measures, Fig. 3(a)) is compared to the case in which a SBW of width w = 3 m is placed 3 m in front of the foundation, so as to intercept the propagating fault rupture. If successful, the SBW will lead to deviation of the fault rupture, and thereby to substantial decrease of foundation rotation and flexural distress.

A combination of experimental and numerical work strengthens the validity of the derived conclusions. Reduced–scale physical model testing is conducted to confirm the effectiveness of the concept, and to offer verification of the numerical modelling. The validated model is subsequently used to conduct a parametric study on the effect of the location of the foundation relative to the fault rupture. Finally, a sensitivity study is conducted to highlight the possible limitations of the proposed mitigation technique.

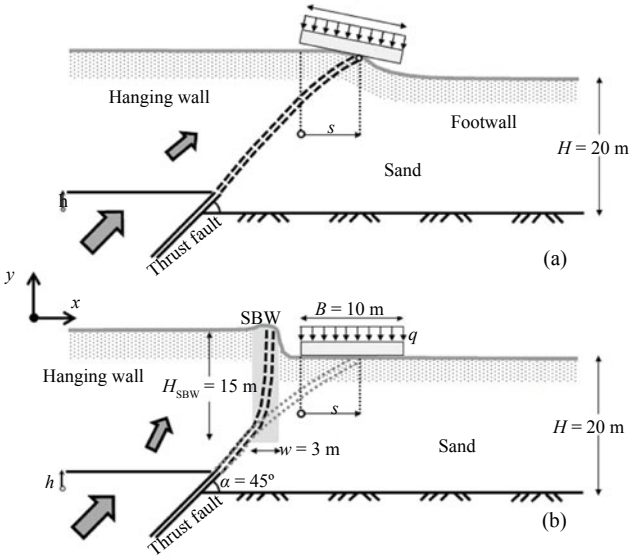

Fig. 3 Sketch of the problem and its geometry: (a) interaction of a thrust fault rupture, propagating through an H = 20 m soil deposit, with a slab foundation of width B, carrying a surcharge load q, positioned at distance s from the theoretical point of rupture outcropping in the free field; and (b) placement of soil bentonite wall (SBW) leads to fault rupture diversion and mitigation of the hazard

2.1 Reduced–scale physical modeling

The device for 1 g testing was built in geotechnical laboratory of IIEES with steel frame using a custom fabricated split-box capable of simulating dip slip (i.e., normal and reverse) faulting and its interaction with shallow foundations. The split-box is 180 cm in length and 50 cm in width, allowing a maximum soil depth of 60 cm (see Fig. 4). An electric actuator was used to push the movable part (0.4 m in length) of the apparatus (representing the hanging wall) up, simulating thrust faulting. The dip angle $\alpha = 45^{o}$, was used for the

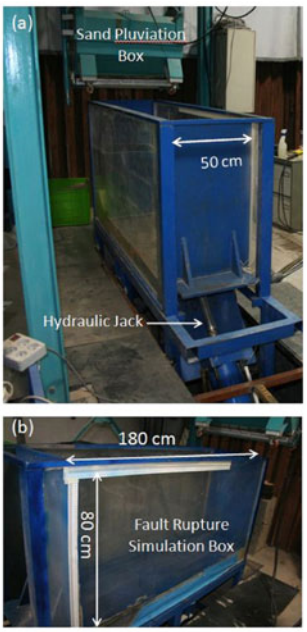

Fig. 4 Photo of split-box

experiments reported herein. Taking its capacity into account, a scale $N = 100$ was selected for the experiments (i.e., the $H = 20$ m prototype soil was modelled as a 20 cm soil layer in the experiments). The $B = 10$ cm foundation (corresponding to the 10 m prototype) was made of Perspex, which is reasonably stiff and adequately light at the same time. The main scope of the experiments was to confirm (at least qualitatively) the effectiveness of the proposed mitigation technique.

The tests were conducted under quasi-static displacement (i.e., at a very slow rate), as essentially happens in reality.

2.1.1 Model preparation

The soil layer was prepared by dry air pluviation of No. 161 Fkooh sanda (relatively) uniform fine sand with a mean grain size d_{50} =0.25 mm, specific weight $G_s = 2.61$, and minimum and maximum dry densities 1.71 g/cm^3 and 1.42 g/cm^3, respectively. The sand was pluviated from a specific height with a fixed sieve aperture to control the mass flow rate, giving a uniform density $D_r \approx 60\%$. The same sand, dyed blue, was used as a marker at the two side walls of the split-box. Direct shear tests were conducted to measure the peak and residual strength of the sand. For $\sigma_v \geq 100$ kPa (representative for the prototype), the peak and residual friction angles were $\varphi_{peak} = 32°$ and $\varphi_{res} = 30°$, while the dilation angle ψ, which depends significantly on the effective stress was approximately 3° for the same normal stress. For low normal stress, $\sigma_v < 10$ kPa, which is more representative of the stress level prevailing in the reduced-scale tests under and around the foundation, the peak friction angle increases substantially, reaching $\varphi_{peak} \approx 45^0$ (see Lade *et al.*, 1984 ; Anastasopoulos *et al.*, 2010).

Fig. 5 1 g model test (a) putting two steel plates in the box; (b) sand pluviation up to 5 cm; (c) the space between two plates filled with clay (clay height is 15 cm); (d) filling the box with sand; and (e) sand and clay wall after two steel plates carefully extracted

The material of the experimental SBW was a clay mixture, consisting of kaolinite and sodium montmorillonite at a 3:1 ratio. At first, two steel plates are placed in the box at the desired locations. The space between these two plates is set according to the desired wall thickness. The sand is poured to the required depth (i.e., 5 cm) and then clay is filled between the two plates. The rest of the box is filled with sand. Finally, the two plates are carefully extracted and the slab foundation is positioned at the desired location (Fig. 5).

Naturally, the properties of the SBW are time dependent. Initially, during backfill placement, the clay mixture is at a liquid state. It then gradually consolidates, attaining its final shear strength in the first few months after construction. According to the literature (Baxter, 2000; Evans and Ryan, 2005), it may be conservatively assumed that the final undrained shear strength S_u can be estimated on the basis of normally consolidated samples. Based on the results of consolidated undrained (CU) tests of such samples, combined with empirical correlations from the literature (Koutsoftas and Ladd, 1985; Look, 2007), the undrained shear strength of the utilized clay mixture was estimated as $S_u / \sigma_v' = 0.25$, leading to an average $S_u \approx 0.3$ kPa. A secant *Young modulus* $E/S_u = 300$ was considered appropriate.

2.1.2 Image processing and instrumentation

To compare the effectiveness of the proposed method, some important response measures are tracked, such as:

- Foundation rotation
- Separation between foundation and soil
- Rupture path in the soil, and
- Surface profile (especially in free field tests)

Measurements were performed with an image processing technique and/or digital instruments. Specifically, fault offset and foundation rotation was measured with both of the above techniques, while soil deformation, rupture path, separation of foundation, and surface profile were assessed only with image processing.

To allow direct observation of the deformed soil, two Plexiglas windows were installed at the two faces of the split-box. Digital images of the deformed soil specimen were captured at every 2 mm of imposed base offset, using a high-resolution (8 MP) digital camera. A series of digital images were collected as the faulting tests proceeded.

All images were rectified using the derived optical parameters of the whole system (camera property, Plexiglas, etc). In Figs. 6(a), (b) two images before and after calibration are shown. Note that in Fig. 6(b) the lengths are real; they can be measured directly from the picture after the scale of this image is determined. Subsequently, when all images are rectified, by computing the optical flow between each pair of consecutive rectified images of the sequence, the relative

motion of sand particles is found in time and space. By tracing the relative motion back to the initial image, the absolute position of sand particles can be computed. For foundation rotation and translation, two red circles above the foundation are constantly being traced. Once the position of these two circles is known, the foundation rotation and translation are computed (see Fig. 6(c)).

Using a Lagrangian description for modelling a motion path, the absolute positions of sand particles are used to obtain the strain field across the image domain. To validate the image processing results, the foundation rotation is determined from both the digital rotation meter above the foundation and from the image processing technique. Comparisons showed that the outcome of the image processing is satisfactory. Vertical displacement of the hanging wall also compared favorably with image processing.

2.2 Numerical simulation

The problem was numerically simulated employing the finite element (FE) method. Despite some shortcomings in accurately modeling shear band formation, FE modelling has been shown to be capable of efficiently reproducing fault rupture propagation in the free field (e.g., Anastasopoulos *et al*., 2007), as well as under shallow and deep foundations (Anastasopoulos *et al*., 2009), and pipelines. A necessary prerequisite is the adoption of a refined mesh (Bray, 1990) and of an appropriate constitutive model for soil. Following the findings of previous studies (Anastasopoulos *et al*., 2007), an elastoplastic constitutive model with Mohr-Coulomb failure criterion and isotropic strain softening was adopted and encoded in ABAQUS (2011). Strain softening is introduced by reducing the mobilized friction angle φ_{mob} and the mobilized dilation angle ψ_{mob} with the increase of plastic octahedral shear strain:

$$\varphi_{mob} = \begin{cases} \varphi_p - \dfrac{\varphi_p - \varphi_{res}}{\gamma_f^p}\gamma_{oct}^p, & \text{for } 0 \le \gamma_{oct}^p < \gamma_f^p \\ \varphi_{res}, & \text{for } \gamma_{oct}^p \ge \gamma_f^p \end{cases} \quad (1)$$

$$\psi_{mob} = \begin{cases} \psi_p \left[1 - \dfrac{\gamma_{oct}^p}{\gamma_f^p}\right], & \text{for } 0 \le \gamma_{oct}^p < \gamma_f^p \\ \psi_{res}, & \text{for } \gamma_{oct}^p \ge \gamma_f^p \end{cases} \quad (2)$$

where: φ_p and φ_{res} are the peak mobilized friction angle and its residual value; ψ_p is the peak dilation angle; and γ_f^p is the plastic octahedral shear strain at the end of softening. To account for the scale effects (Muir Wood, 2004), an approximate simplified scaling method is employed for γ_f^p, as described in Anastasopoulos *et al*. (2007) along with the procedure for calibrating the model parameters. Pre-yield behavior is modeled as linear elastic, with a secant modulus $G_s = \tau_y/\gamma_y$ that linearly increases with depth.

The problem is analyzed in 2D assuming plane strain conditions. The soil is modelled with quadrilateral continuum elements of dimension $d_{FE} = 0.5$ m to achieve a reasonably refined mesh (Anastasopoulos *et al*., 2007). The slab foundation, modelled with linear elastic beam elements, is positioned on top of the soil model and connected to it through special contact elements, which are rigid in compression but tensionless, allowing detachment of the foundation from the bearing soil (i.e., gap formation beneath the foundation). Whenever positive normal force is transmitted, the interface shear obeys Coulomb's friction law, allowing for slippage. Both detachment and slippage are important phenomena for realistic foundation modelling in this case.

The bottom boundary of the model represents the interface between the soil and the underlying bedrock. Hence, it is split in two parts, one remaining stationary and representing the footwall, and the other one being subjected to the movement of the hanging wall. The large deformation Lagrangian description was adopted because of the large imposed dislocation.

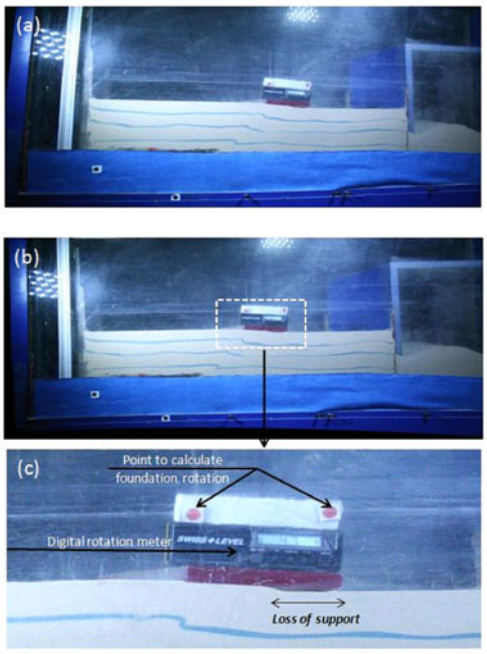

Fig. 6 Photo of split-box during the test: (a) distorted image; (b) rectified image; and (c) close view of foundation and digital rotation meter above. Note that the perspective changes between image (a) and (b)

3 Effectiveness of the soil bentonite wall

The effectiveness of the proposed seismic hazard mitigation technique is explored for a lightly-loaded surface foundation. The results of reduced–scale physical model tests are compared with FE analysis results, offering combined evidence on the performance of the SBW, and additional verification of the numerical analysis method employed herein. The latter has been

extensively validated through Class "A" predictions of centrifuge model tests referring to: normal and reverse fault rupture propagation in the free field, interaction of a propagating fault rupture with rigid and flexible surface foundations, and rigid caisson foundations subjected to normal and reverse faulting (Anastasopoulos *et al*., 2007 and 2009).

3.1 Fault rupture propagation in the free field

Results from the free field test are discussed first as a reference for the interaction tests (Fig. 7). The deformed soil model with superimposed displacement vectors (as computed through image processing) is compared with the deformed FE mesh, for bedrock fault offset h = 2 m (Fig. 7(a)). Unless otherwise stated, all results are in prototype scale. The analysis appears to agree qualitatively with the experiment, predicting with reasonable accuracy the rupture path and the location of its emergence on the ground surface.

This is further confirmed in Fig. 7(b), which compares the experimental and analyical results in terms of vertical displacement profiles of the ground surface, for a range of fault offset at bedrock. While the FE results are plotted for h = 1.0, 1.4 and 2.0 m (exactly), the experimental images were obtained for roughly the same bedrock offset: h = 0.9, 1.35, and 2.1 m. A quite satisfactory agreement is observed for all three examined fault dislocations. The only discrepancy refers to the gradient of the surface scarp near the crest, which appears smaller in the numerical model (something which is also observable in Fig. 7(a)). This discrepancy is attributable to the very low confining pressures in the reduced-scale (1 g) experiment, and the associated increased friction and dilation angle (compared to prototype conditions), and the simplified modelling of post peak soil behavior.

3.2 Fault rupture–soil–foundation interaction

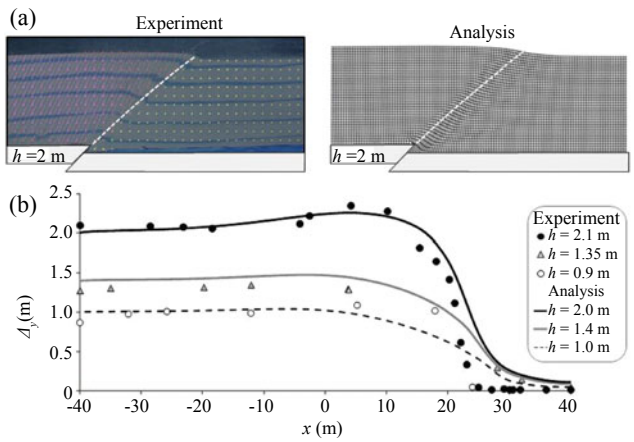

Fig. 7 Free-field thrust fault rupture propagation through loose sand. Comparison of experimental with numerical analysis results: (a) photo of the deformed model with superimposed displacement vectors computed through image analysis, compared to FE deformed mesh for bedrock fault offset h = 2 m; and (b) vertical displacement profiles at the soil surface for three fault offset amplitudes

To focus on the effectiveness of the SBW, a light uniform surcharge load q = 20 kPa was used in the experiments (so that the observed fault rupture diversion can be solely attributed to the presence of the SBW. With respect to its location relative to the unperturbed fault rupture, the B = 10 m foundation is positioned at s = 7 m (or s/B = 0.7 in dimensionless terms) to investigate a worst-case scenario: the fault rupture would outcrop very close to the middle, imposing substantial flexural distortion and rotation (see Anastasopoulos *et al*., 2010). The performance of the foundation for the unprotected case is compared with the proposed seismic hazard mitigation provided by the construction of a SBW.

The results for the unprotected case are summarized in Fig. 8. The image of the deformed soil specimen with superimposed displacement vectors compares reasonably well with the FE deformed mesh, for bedrock fault offset h = 2 m (Fig. 8(a)). Due to the relatively light bearing pressure of the foundation, the rupture trace is quite similar to that in the free-field. While in the experiment an area of loss of support (i.e., a gap underneath the foundation) can be clearly observed, the numerical analysis seems to predict a somewhat milder soil deformation. Again, this qualitative difference could be attributed to modelling inaccuracies given the low confining stresses in the experiment, due to which the loose sand tends to behave in a more brittle manner. Despite this difference, the numerical prediction is again in good agreement with the experiment regarding the foundation rotation θ (Fig. 8(b)).The latter reaches almost 5.5° for bedrock fault offset h = 2 m (or h/H = 10% in dimensionless terms), a value well beyond acceptable limits in terms of functionality of the supported structure—an issue of great concern in the sequel.

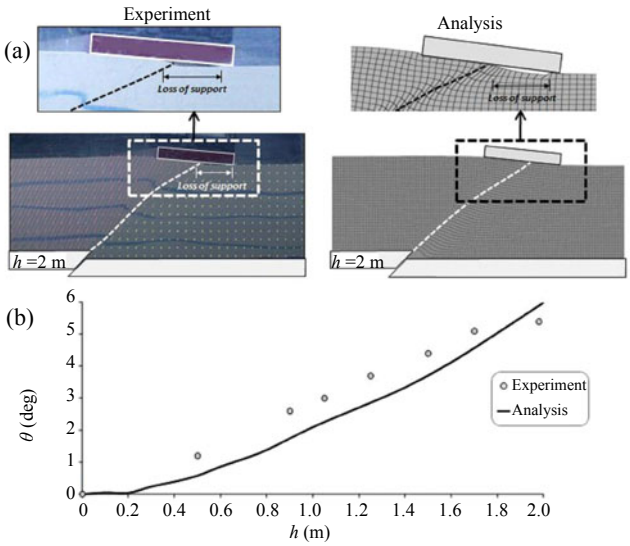

Fig. 8 Interaction of a reverse fault rupture propagating through loose sand with a B = 10 m foundation positioned at s = 7 m. Comparison of experimental with numerical analysis results: (a) photo of the deformed model with superimposed displacement vectors computed through image analysis, compared to FE deformed mesh for bedrock fault offset h = 2 m; and (b) evolution of foundation rotation θ with imposed fault offset h

The role of the soil bentonite wall (SBW) placed in front of the foundation to intercept the rupture path, as envisaged in the sketch of Fig. 3, is now revealed in Fig. 9. Both the experiment (left) and the analysis (right) demonstrate the effectiveness of the intervention. While the foundation position, width, and surcharge load are identical to the unprotected case of Fig. 8, the SBW successfully absorbs most of the faulting–induced compression, effectively diverting the fault rupture upwards before reaching the foundation. Numerical analysis and experimental results are in full accord. The foundation is almost unaffected by the fault rupture, maintaining full contact with the bearing soil (no gapping is observed), and hence not subjected to any measurable flexural distress (as will be shown later on). Moreover, with the foundation remaining on the footwall practically unaffected by the upward offset of the hanging wall, the resulting foundation rotation θ is also substantially reduced, from about 6° to less than 2° for h = 2 m (compare Fig. 9(b) with Fig. 8(b)). It is interesting to notice in Fig. 9 the substantial compression imposed by thrust faulting, in effect a passive loading, the deformations from which are absorbed by the SBW. As a consequence, the thickness of SBW reduces from the initial 3 m to less than 1 m at its deepest, when the bedrock fault offset reaches h = 2 m. Evidently, such a non-trivial wall thickness (3 m) is one of the key factors for the observed success of the intervention.

4 Parametric numerical study

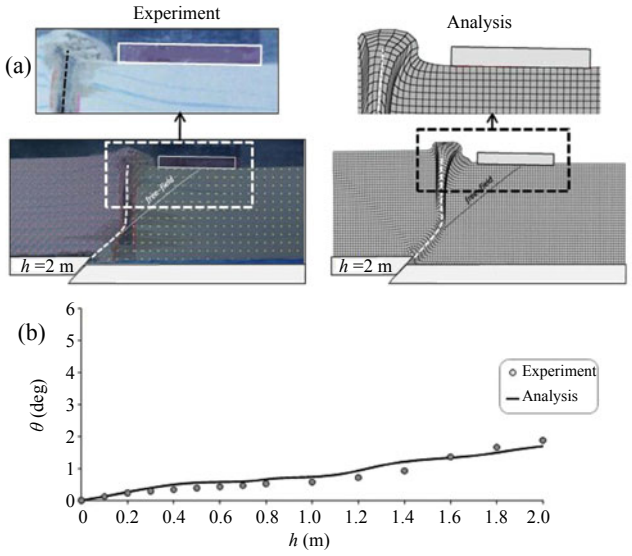

Fig. 9 Interaction of a reverse fault rupture propagating through loose sand with a B = 10 m foundation positioned at s = 7 m and protected with a soil bentonite wall (SBW). Comparison of experimental with numerical analysis results: (a) photo of the deformed model with superimposed displacement vectors computed through image analysis, compared to FE deformed mesh for bedrock fault offset h = 2 m; and (b) evolution of foundation rotation with imposed fault offset h

The encouraging results of Fig. 9 for the effectiveness of the SBW motivated the following detailed theoretical parametric study in support of the validity of the proposed seismic hazard mitigation technique.

Although all of the analyses are conducted for an H = 20 m soil deposit of sand and a B = 10 m foundation, the key results and conclusions are of more general validity. As suggested by Berill (1983), Cole and Lade (1984), and Bray (1990), and in accord with the principles of dimensional analysis (e.g., Muir Wood, 2004; Palmer, 2008), the deformation field can be normalized to the soil thickness H. Hence, the bedrock fault offset h and the vertical displacement Δy can be written non-dimensionally as h/H and $\Delta y/H$. Although scale effects tend to complicate the problem, rendering this normalization not strictly accurate, it has been shown by Anastasopoulos *et al*. (2007) to offer a reasonable engineering approximation. Correspondingly, the foundation bending moment M and the surcharge load q are expressed in non-dimensional form as M/qB^2 and $q/\rho gB$, respectively. The dip angle α is always 45° and the raft foundation is rigid.

The following parameters are parametrically investigated:

(a) The location of the foundation relative to the free-field fault outcrop (measured from its hanging-wall edge): s = 1 to 11 m, or in dimensionless form: s/B = 0.1 to 1.1.

(b) The dead load of the superstructure, expressed in the form of a uniformly distributed surcharge load q = 20, 40, and 80 kPa (representative values for 1, 3, 5-story buildings), or in dimensionless form: $q/\rho gB$ = 0.1, 0.2 and 0.4.

Their impact on the effectiveness of the SBW in protecting the foundation–structure system is outlined in the sequel. The width (w = 3 m), location (3 m in front of the foundation), and the depth (15 m) of the SBW are kept constant.

4.1 Significance of the fault rupture location, *s/B*

First, three characteristic locations (s/B = 0.1, 0.5, and 0.9) are studied in detail with respect to the effectiveness of the SBW, focusing on the higher surcharge loads ($q/\rho gB$ = 0.2, 0.4). The results of the SBW–protected foundation are compared to the unprotected case.

Faulting at *s/B* = 0.1

In this case, the free field fault rupture would have outcropped close to the left edge of the foundation. The results are presented in terms of deformed mesh and vertical displacement profile of the ground surface (Fig. 10), as well as normalized foundation contact pressure p/q and bending moment M/qB^2 distributions (Fig. 11).

Evidently, the SBW absorbs most of the faulting–induced deformations by being heavily compressed (and hence upwardly extruded) and sheared. As a result, the fault rupture is "arrested" inside the wall, hardly affecting the ground deformation behind or in front of it.

The foundation experiences a much reduced rotation and does not suffer any loss of contact with the supporting soil. By contrast, the unprotected foundation undergoes intolerable rotation and loss of contact, at least for the largest fault offset examined (h = 2 m).

These are further confirmed from the evolution of the normalized contact pressures p/q and foundation bending moments M/qB^2 (Fig. 11). Under the initial static loading, before imposing the tectonic dislocation, the foundation is of course in full contact with the bearing soil and a rather negligible maximum bending moment M_o is observed at mid-span. In fact, with a "Gibson" soil (i.e., one with undrained modulus proportional to depth), or equivalently with a Winkler medium, the static moment would be exactly zero (Gibson and Kalsi 1974; Gazetas, 1983). In the unprotected case (left column), the rupture emerges underneath the foundation for bedrock fault offset h/H = 3%, leading to a substantial reduction of the contact pressures near the middle. As a result, the foundation experiences a substantial bending moment M/qB^2_{max} = 0.06 – nearly three times larger than the static M_o. With h/H = 5%, complete loss of support under 1/3 of the contact area does not lead, surprisingly, to increased M/qB^2.

With the installation of SBW, the foundation performance (right column), is drastically improved. With the fault rupture being effectively arrested inside the wall, which acts as a weak in shear and compressible "barrier," both contact pressures and bending moment are essentially unaffected by the imposed tectonic deformation (the bending moment increases by 40%, at most, for h/H = 5%).

Faulting at s/B = 0.5

The results for this case, in which the free-field (unperturbed) fault rupture would have emerged near the middle of the foundation, are summarized in Fig. 12. Quite similarly with the previous case, the SBW absorbs the faulting–induced deformation, compressed and squeezed up, thereby minimizing the ground distortion affecting the foundation. Loss of support is avoided and flexural distress is limited. On the other hand, the unprotected foundation experiences loss of support (from x/B = 0.65 to 0.75), already for bedrock offset h/H = 3%, and increased bending moment (2.6M_o).

Although no shear band emerges beyond the SBW, the closer proximity of the foundation to the fault compared to the previous case (s/B = 0.1), does induce some ("leaking") deformation under the foundation. Hence, the contact pressures are a little more sensitive to variations in h, especially near the edges, and the bending moments increase by up to 70% over the initial (pre-seismic) value M_o for h/H = 5%.

Faulting at s/B = 0.9

In this case (Fig. 13), the free field unperturbed fault rupture would have emerged near to where the right edge of the foundation is now. The successful performance of the SBW in absorbing the thrust of the fault and protecting the foundation from significant rotation and flexural distress is evident, and is essentially insensitive to the fault offset (at least for h/H up to 5%). So is the similarity in contact pressures and bending moments with the s/B = 0.5 case. By contrast, the unprotected foundation is highly sensitive to the bedrock fault offset h. As h increases, the foundation is subjected to an increasingly–hogging deformation. The result: the contact pressures under the left edge continue to diminish, until at h/H = 5%, the edge completely detaches from the soil, the foundation support moves towards the middle, and the bending moments reverse in sign. Not only is the maximum M/qB^2 almost 2.2 times larger than the static moment M_o, but – most importantly – it now acts in the opposite direction of what would have been expected for static loads.

Performance in terms of foundation rotation

So far, the SBW seismic mitigation scheme has been proven to be quite successful in reducing the foundation distress, for all fault rupture locations examined. Reducing the foundation bending moments can be seen

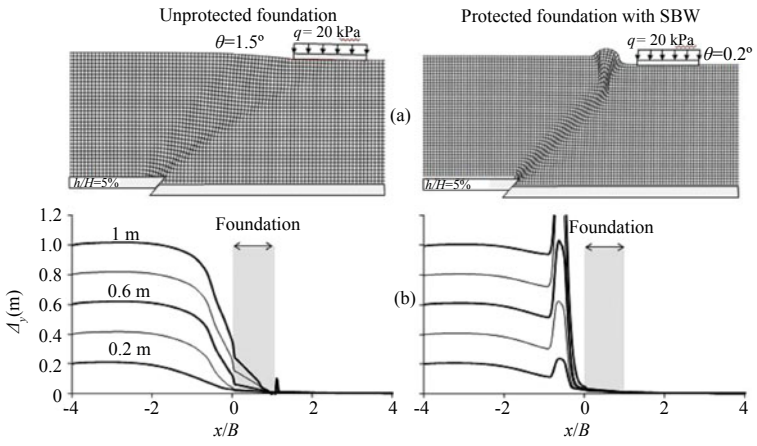

Fig. 10 Effectiveness of fault hazard mitigation with a w = 3 m *Soil Bentonite Wall* (SBW) for a B = 10 m foundation carrying q = 20 kPa surcharge load, positioned at distance s/B = 0.1. Comparison of the unprotected case (left) with the SBW (right): (a) deformed mesh for h/H = 5 %; and (b) vertical displacement profile at the ground surface

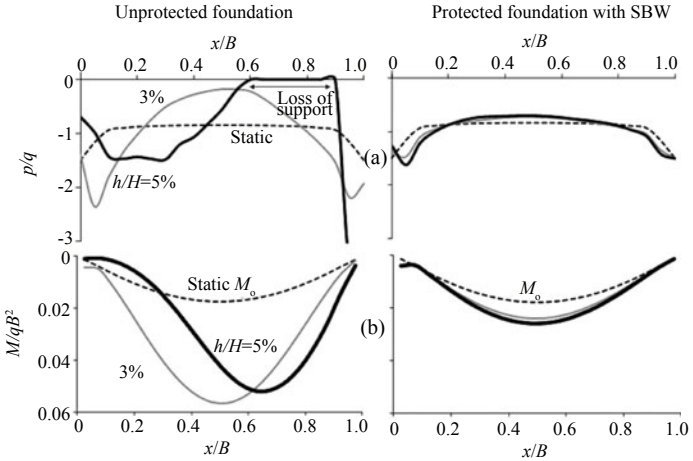

Fig. 11 Effectiveness of fault hazard mitigation with a w = 3 m *Soil Bentonite Wall* (SBW) for a B = 10 m foundation carrying q = 20 kPa surcharge load, positioned at distance s/B = 0.1. Comparison of the unprotected case (left) with the SBW case (right): (a) normalized contact pressures p/q along the width of the foundation; and (b) normalized foundation bending moment M/qB^2 along the width of the foundation

as a measure of effectiveness for the survival of the foundation–structure system (avoidance of differential settlement and hence collapse). Serviceability of the structure, however, requires minimal post-seismic rigid-body rotation of the foundation.

To better visualize the effectiveness of the SBW in terms of reduction of rigid body rotation, Fig. 14 compares the evolution of foundation rotation θ with fault offset h, for the unprotected foundation and the SBW–protected system. The differences are indeed quite striking: installation of the SBW reduces the foundation rotation to a little more than just 1/10 of the value to be experienced by the unprotected foundation — quite a remarkable performance.

4.2 Increasing the load from the superstructure

The significance of the load transmitted onto the soil is explored by parametrically varying the magnitude of the surcharge load: q = 20, 40, and 80 kPa (In dimensionless terms: $q/\rho gB$ = 0.1, 0.2, and 0.4). All fault positions are considered: s/B = 0.1 to 0.9. Due to space limitations, detailed results are shown in Fig. 15 only for $q/\rho gB$ = 0.2 and s/B = 0.5.

Contrasting with Fig. 13, it can be readily seen that the increase of the surcharge load has a beneficial effect on foundation distress. The effect is particularly conspicuous in the unprotected foundation case: increasing $q/\rho gB$ leads to further diversion to the left of the secondary branch of the fault rupture, and

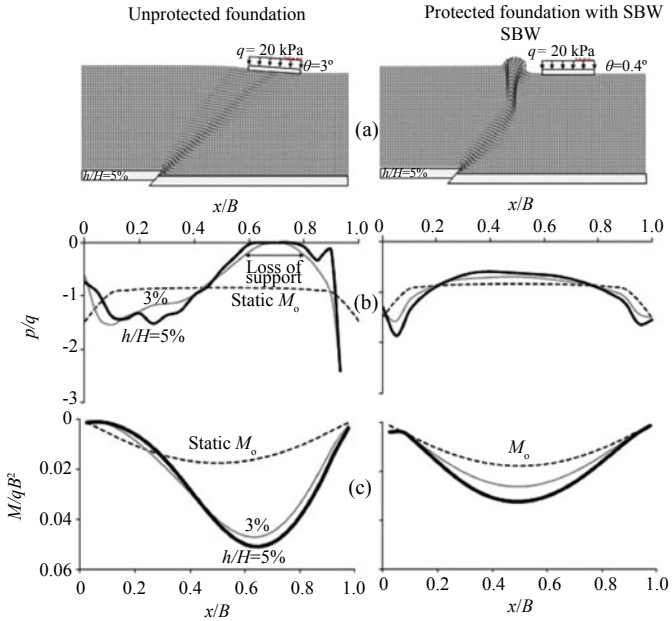

Fig. 12 Effectiveness of fault hazard mitigation with a w = 3 m *Soil Bentonite Wall* (SBW) for a B = 10 m foundation carrying q = 20 kPa surcharge load, positioned at distance s/B = 0.5 (i.e., s = 5 m). Comparison of the unprotected case (left) with the SBW (right): (a) deformed mesh for h/H = 5%; (b) normalized contact pressures p/q along the width of the foundation; and (c) normalized foundation bending moment M/qB^2 along the width of the foundation

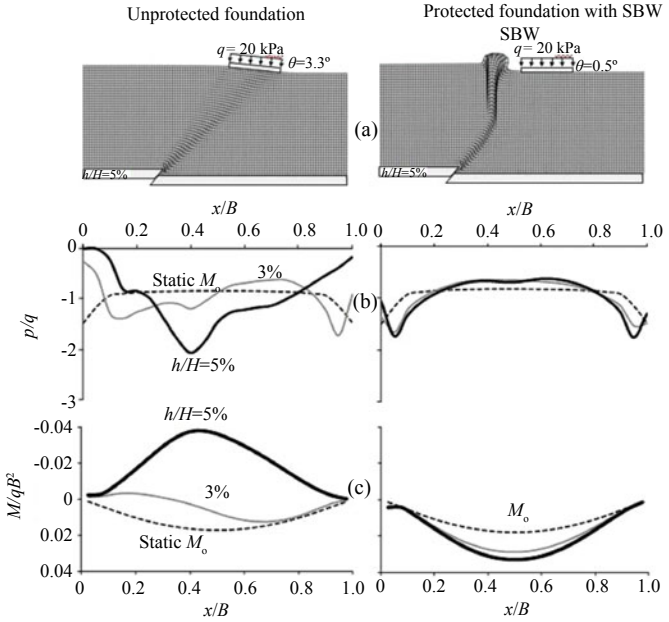

Fig. 13 Effectiveness of fault hazard mitigation with a w = 3 m *Soil Bentonite Wall* (SBW) for a B = 10 m foundation carrying q = 20 kPa surcharge load, positioned at distance s/B = 0.9 (i.e., s = 9 m). Comparison of the untreated case (left) with the SBW (right): (a) deformed mesh for h/H = 5%; (b) normalized contact pressures p/q along the width of the foundation; and (c) normalized foundation bending moment M/qB^2 along the width of the foundation

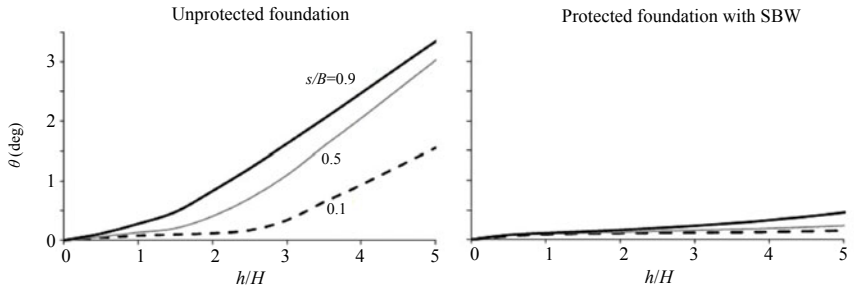

Fig. 14 Summary of parametric numerical results in terms of foundation rotation θ as a function of normalized fault offset h/H for s/B = 0.1, 0.5, and 0.9: comparison of the unprotected with SBW–protected foundation

substantial flattening of the ground surface under the foundation. Hence, loss of support is practically cancelled and flexural distress substantially reduced. In fact, the interaction mechanism is quite different, as the foundation is now subjected to hogging instead of sagging deformation. Observe the complete reversal of M/qB^2 for h/H = 5%. Despite the previously discussed problems of such moment reversal, the maximum M/qB^2 is only about 0.6 M_o, small enough not to be of major concern.

With SBW protection, the foundation is almost insensitive to the imposed tectonic deformation up to 5% of fault dislocation. This is especially so for bending moments and rotation; contact pressures exhibit a small dependence on h.

An overall picture of the role of the surcharge load $q/\rho gB$ carried by the foundation in the development of bending moment distributions and in the improvement caused by installing a SBW is given in Fig. 16, in terms of normalized foundation bending moment M/qB^2 envelopes (i.e., only the absolute largest and smallest values of M/qB^2 are recorded) for all fault rupture locations (s/B = 0.1 to 0.9) and fault offset h/H ranging from 0 to 5%. For reference, the static moment diagram is also plotted in the figure. The following remarks are worthy of note:

- SBW protection works very well regardless of applied surcharge load.
- The unprotected foundation performs poorly when the applied pressure is quite small ($q/\rho gB$ = 0.1), but it improves significantly with increasing pressure.
- At high applied pressures ($q/\rho gB \geq$ 0.4) even the performance of the unprotected foundation is structurally satisfactory and, hence, the need for the SBW to reduce the foundation flexural distress diminishes. However, in terms of foundation rotation, this is not the case at all. Indeed, as Fig. 17 vividly demonstrates, despite the beneficial effect of increased foundation pressure in reducing the rotation of the unprotected foundation, the latter still may reach values of up to 2.8° for the h/H = 5%. The improvement achieved thanks to *SBW* is quite significant and would justify its use for meeting even stringent serviceability criteria.

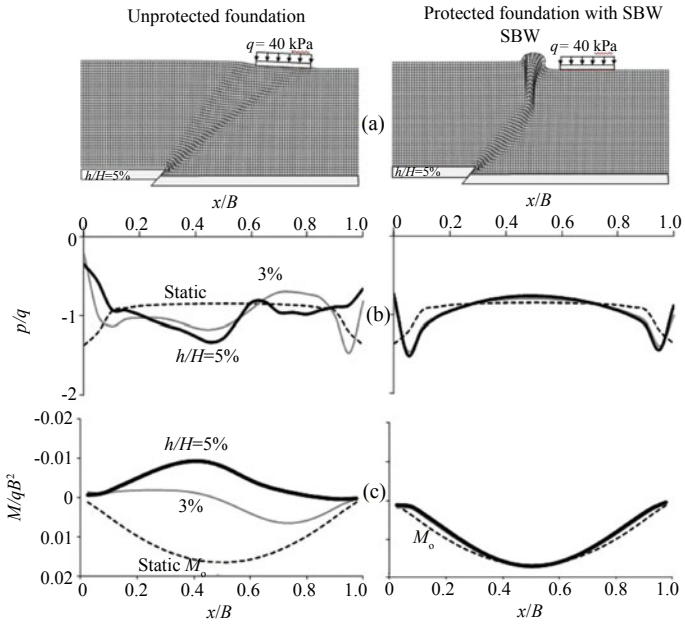

Fig. 15 Importance of increased surcharge load q = 40 kPa on the effectiveness of fault hazard mitigation through w = 3 m *Soil Bentonite Wall* (SBW) for a B = 10 m foundation at distance s/B = 0.5. Comparison of the unprotected case (left) with the SBW (right): (a) deformed mesh for h/H = 5%; (b) normalized contact pressures p/q along the width of the foundation; and (c) normalized foundation bending moment M/qB^2 along the width of the foundation.

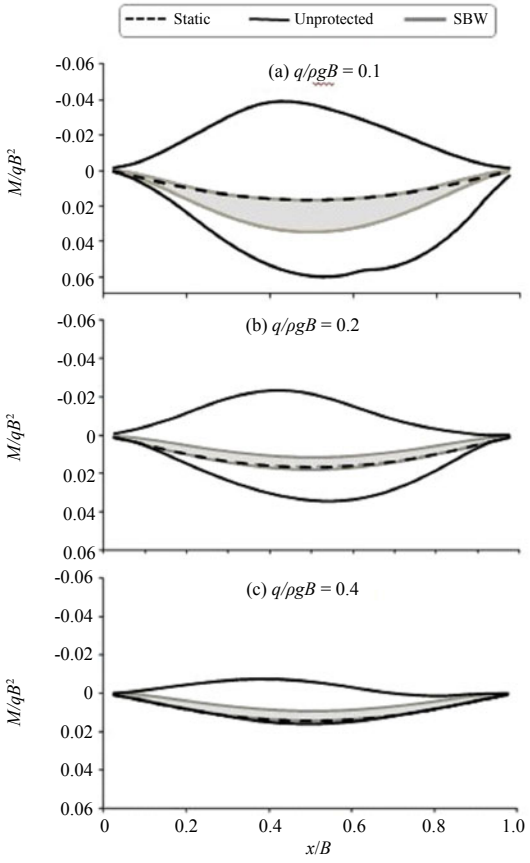

Fig. 16 The effect of the magnitude of surcharge load $q/\rho gB$ on the effectiveness of *Soil Bentonite Wall* (SBW): envelopes of foundation bending moment M/qB^2 for all fault rupture locations (s/B = 0.1 to 0.9) and fault offset h/H ranging from 0 to 5% for normalized surcharge load

5 Conclusions and limitations

A novel seismic hazard mitigation technique has been explored, aiming to protect foundation–structure systems from a thrust fault that may rupture underneath. This is achieved through a weak wall "barrier," placed

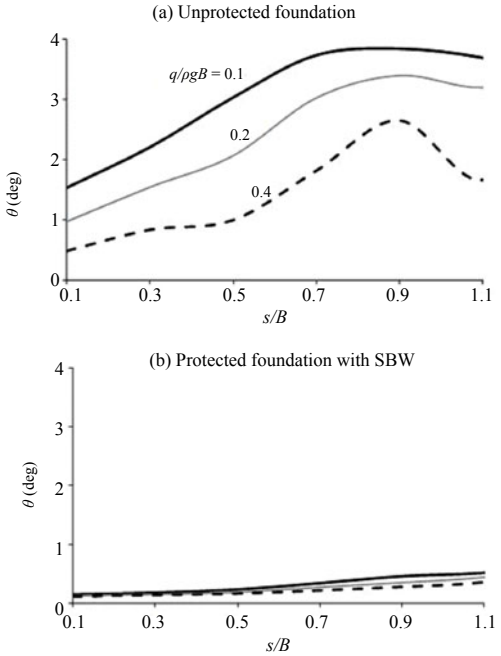

Fig. 17 Effect of the fault rupture locations and surcharge load on the effectiveness of the *Soil Bentonite Wall* (SBW) in terms of foundation rotation. Comparison between: (a) the unprotected case; with (b) mitigation through addition of SBW

between the outcropping dislocation and the foundation. A specific case has been examined, referring to a B = 10 m rigid slab foundation, lying on a 20 m thick sandy soil layer, the base of which undergoes tectonic dislocation. The weak wall "barrier" is materialized through a w = 3 m thick *Soil Bentonite Wall* (SBW), constructed at a distance of w = 3 m in front of the structure, and having a depth of H_{SBW}= 15 m so that it intercepts the rupture path for the specific case examined herein.

The paper has presented a numerical parameter study, supported by a number of reduced–scale physical model tests, exploring the effectiveness of the proposed SBW mitigation technique. It is shown that installing a SBW is indeed quite an effective hazard mitigation method. Thanks to its small shear strength and large capacity to be compressed, the SBW "absorbs" the thrust, diverting the fault rupture upwards and saving the foundation from a direct "hit." As a result, the flexural distress and especially the rigid body rotation of the foundation are negligibly small, even when the fault offset is as high as 5% of the soil layer thickness.

By contrast, the unprotected foundation experiences larger flexural distress and, more significantly, much larger (and mostly intolerable) rotation. Of course, when the foundation is heavily loaded, its flexural distress may be acceptably small (even if unprotected), but its rotation still threatens the serviceability of the structure. This beneficial effect of increased foundation pressure is the outcome of two complementary phenomena: (a) the increase of the compressional stress field underneath the foundation causes an increasing diversion of the fault rupture away from the foundation, towards less compressed and hence easier to shear region; and (b) the increase of compression of the surface of supporting soil smoothens the faulting-induced scarps or anomalies of the ground surface and hence makes the contact pressure more uniform.

Evidently, with a heavy transmitted load from a tall superstructure, the need or not for protection by means of SBW will be decided on the basis of predicted rotation and not on the imposed distress on the foundation.

The results presented herein are valid for the specific thickness of soil stratum (H = 20 m), soil density ($D_r \approx 60\%$), fault dip angle (α = 45°), and geometric and material characteristics of the SBW (w =3 m, H_{SBW}=15 m, undrained shear strength $S_u/\sigma_v' = 0.25$). Moreover, the fault offset was restricted to $h/H \leq 5\%$. The derived conclusions may differ substantially when some of the above variables are different. For instance, if the soil layer is substantially thicker than 20 m, much greater fault offset is required to produce substantial fault scarp at the ground surface. Hence, implementing such a protective measure may not be as indispensable as was the case in this paper.

The magnitude of fault offset is critically important. As discussed herein, the SBW may absorb a fault offset of up to 5%. The effect of further increasing the fault offset to h/H = 10% is summarized in Fig. 18. Increasing the fault offset h/H, the benefit from the SBW is reduced significantly in terms of contact pressures and bending moments. Apparently, to maintain satisfactory performance of the SBW protected foundation, a thicker wall would be needed to accommodate the larger lateral compressional deformation. Nevertheless, even in this case, the SBW provides an invaluable contribution towards minimizing the rotation of the foundation (Fig. 19).

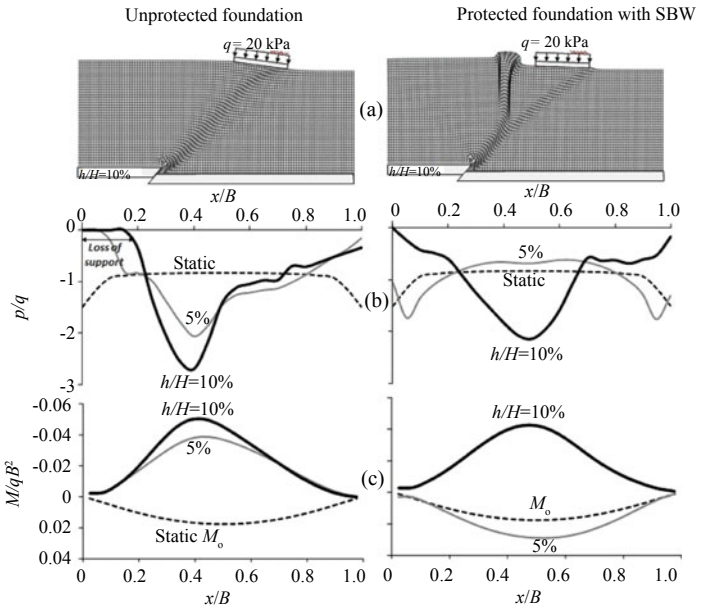

Fig. 18 Comparison of the response of the unprotected foundation (left column) with the response of the SBW-protected (left column) in the case of s/B = 0.9 for h/H = 5 % and 10% From top to bottom : (a) deformed mesh; (b) normalized contact pressures p/q ; and (c) normalized foundation bending moment M/qB^2; (B = 10 m load $q/\rho gB$ = 0.1)

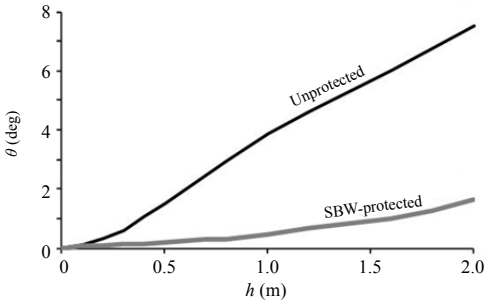

Fig. 19 Comparison of the unprotected with the SBW–protected foundation: evolution of foundation rotation with bedrock fault offset h (H=20 m, B = 10 m, $q/\rho gB$ = 0.1, positioned at s/B = 0.9)

Acknowledgment

The authors (MF, KJ, MK) would like to acknowledge the technical and financial support of IIEES under the research project "Evaluation of possible measures to construct in vicinity of active fault". The National Technical University of Athens authors (IA, GG) acknowledge the financial support under the research project "DARE", by the European Research Council's (ERC) "IDEAS" Programme, in Support of Frontier Research under contract/number ERC–2–9–AdG228254–DARE.

References

Anastasopoulos I, Antonakos G and Gazetas G (2010), "Slab Foundations Subjected to Thrust Faulting: Parametric Analysis and Simplified Design Method," *Soil Dynamics and Earthquake Engineering*, **30**(10): 912–924.

Anastasopoulos I and Gazetas G (2005), "Design Against Fault Rupture: Methodology and Applications in Greece," *Proceedings of the 1st Greece – Japan Workshop: Seismic Design, Observation and Retrofit of Foundations,* Athens, October 11−12, 2005, pp. 345−366.

Anastasopoulos I and Gazetas G (2007a), "Foundation-structure Systems over a Rupturing Normal Fault: Part I. Observations after the Kocaeli 1999 Earthquake," *Bulletin of Earthquake Engineering*, **5**(3): 253−275.

Anastasopoulos I and Gazetas G (2007b), "Behavior of Structure–foundation Systems over a Rupturing Normal Fault: Part II. Analysis of the Kocaeli Case Histories," *Bulletin of Earthquake Engineering*, **5**(3): 277–301.

Anastasopoulos I and Gazetas G (2010), "Analysis of Cut-and-cover Tunnels against Large Tectonic Deformation," *Bulletin of Earthquake Engineering,* **8**(2): 283–307.

Anastasopoulos I, Gazetas G, Bransby F, Davies MCR and El Nahas A (2007), "Fault Rupture Propagation through Sand: Finite Element Analysis and Validation through Centrifuge Experiments," *Journal of Geotechnical and Geo Environmental Engineering*, ASCE, **133**(8): 943−958.

Anastasopoulos I, Gazetas G, Bransby MF, Davies MCR and El Nahas A (2009), "Normal Fault Rupture Interaction with Strip Foundations," *Journal of Geotechnical and Geoenvironmental Engineering*, ASCE, **135**(3): 359–370.

Anastasopoulos I, Gazetas G, Drosos V, Georgarakos T and Kourkoulis R (2008a), "Design of Bridges against Large Tectonic Deformation," *Earthquake Engineering and Engineering Vibration*, **7**(4): 345–368.

Anastasopoulos I, Gerolymos N, Drossos V, Kourkoulis R, Georgarakos P and Gazetas G (2008b), "Behaviour of Deep Immersed Tunnel under Combined Major Fault Rupture and Strong Seismic Shaking," *Bulletin of Earthquake Engineering*, **6**(2): 213–239.

Baxter Y Diane (2000), "Mechanical Behavior of Soil-bentonite Cutoff Walls," *PhD Dissertation,* Virginia Polytechnic Institute.

Berill JB (1983), "Two-dimensional Analysis of the Effect of Fault Rupture on Buildings with Shallow Foundations," *Soil Dynamics and Earthquake Engineering*, **2**(3): 156–160.

Bransby MF, Davies MCR, El Nahas A and Nagaoka S (2008), "Centrifuge Modelling of Reverse Fault-foundation Interaction," *Bulletin of Earthquake Engineering*, **6**(4): 607–628.

Bray JD (1990), "The Effects of Tectonic Movements on Stresses and Deformations in Earth Embankments," *PhD Dissertation*, University of California, Berkeley.

Bray JD (2001), "Developing Mitigation Measures for the Hazards Associated with Earthquake Surface Fault Rupture," *Seismic Fault-induced Failures Workshop*, Japan Society for the Promotion of Science, University of Tokyo, Japan, pp. 55–79.

Cole DA Jr and Lade PV (1984), "Influence Zones in Alluvium Over Dip-slip Faults," *Journal of Geotechnical Engineering*, ASCE, **110**(GT5): 599–615.

Eurocode EC8 (1994), *Structures in Seismic Regions. Part 5: Foundations, Retaining Structures, and Geotechnical Aspects*. Commission of the European Communities, Brussels.

Evans JC, Costa MJ and Cooley B (1995), "The State-of-stress in Soil-bentonite Slurry Trench Cutoff Walls," *Proc., Geo-environment 2000, ASCE Geotechnical Special Publication* No. 46, Y.B. Acar and D. E. Daniel, eds., New Orleans, Louisiana, 1173–1191.

Evans J and Ryan C (2005), "Time-dependent Strength Behavior of Soil-bentonite Slurry Wall Backfill," *Proceedings of the Sessions of the Geo-frontiers ASCE Congress*, January 24–26, Austin, Texas, USA.

Faccioli E, Anastasopoulos I, Callerio A and Gazetas G (2008), "Case Histories of Fault–foundation Interaction," *Bulletin of Earthquake Engineering*, **6**(4): 557–583.

Gazetas G (1983), "Analysis of Machine Foundation Vibrations: State-of-the-art," *Soil Dynamics and Earthquake Engineering,* **2**(1): 2–43.

Gibson RE and Kalsi GS (1974), "The Surface Settlement of a Linearly Inhomogeneous Cross-anisotropic Elastic Half-space," *Z. Angew. Math. Phys.*, **25**: 843–847.

Koutsoftas DC and Ladd CC (1985), "Design Strengths for an Offshore Clay," *Journal of Geotechnical Engineering*, ASCE, **111**(3): 337–355.

Lade PV, Cole DA and Cummings D (1984), "Multiple Failure Surfaces over Dip-slip Faults," *Journal of Geotechnical Engineering*, ASCE, **110**(GT5): 616–627.

Lin A, Ren Z, Jia D and Wu X (2009), **"**Co-seismic Thrusting Rupture and Slip Distribution Produced by the 2008 M_w7.9 Wenchuan Earthquake, China," *Tectonophysics*, **471**: 203–215.

Look Burt G (2007), *Handbook of Geotechnical Investigation and Design Tables*, Taylor & Francis Group, London.

McKnight J, Louay T and Owaidat M (2001), "Quality Control and Performance of a Cutoff Wall for Containment of DANPL Plume," *Proc International Conference on Containment & Remediation Technology*, Orlando.

Muir Wood (2004), *Geotechnical Modeling*, Spon Press., New York, NY

Palmer AC (2008), *Dimensional Analysis and Intelligent Experimentation*, World Scientific Publishing, Singapore.

Paolucci R and Yýlmaz MT (2008), "Simplified Theoretical Approaches to Earthquake Fault Rupture-shallow Foundation Interaction," *Bulletin of Earthquake Engineering*, **6**(4): 629–644.

Ryan C (2007), "Vertical Groundwater Barriers for Contaminated Site Reclamation," *Proc. of the 10th Australia–New Zealand Conference on Geo-Mechanics*, Australia

Yilmaz MT and Paolucci R (2007), "Earthquake Fault Rupture–shallow Foundation Interaction in Undrained Soils: a Simplified Analytical Approach," *Earthquake Engineering and Structural Dynamics*, **36**(1): 101–118.